Figure 12.1 First flight of PX-1 on September 28, 2007

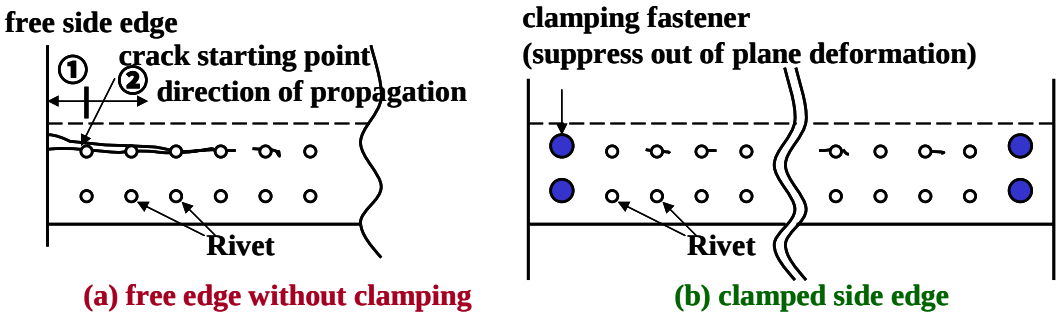

Fig. 12.2 Single Lap Joint Specimen with Double Row Fastener

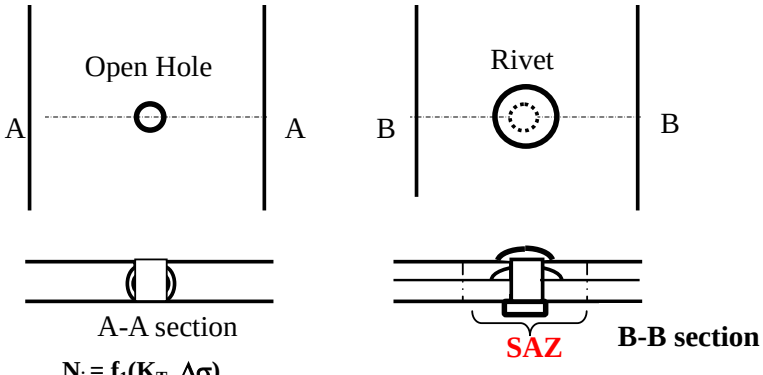

$N_i = f_1(K_T, \Delta\sigma)$

$da/dn = f_2(\Delta\sigma)$

N_i :number of cycles when a crack grows to detectable size

SAZ: Squeezing Affected Zone

$= f(F, t, p, r)$

F: Squeezing force, t: thickness

p: fastener pitch, r: fastener row

$N_i = f_3(\Delta\sigma, F/t, p, r)$, $da/dn = f_4(\Delta\sigma, SAZ)$

Figure 12.3 Difference of open hole and fastener on N_i and da/dn

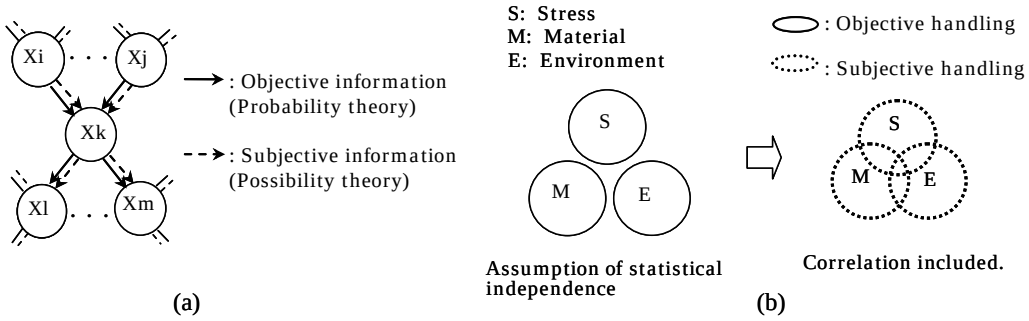

Fig. 12.4 Extended Bayesian Network (a) and Its Advantage

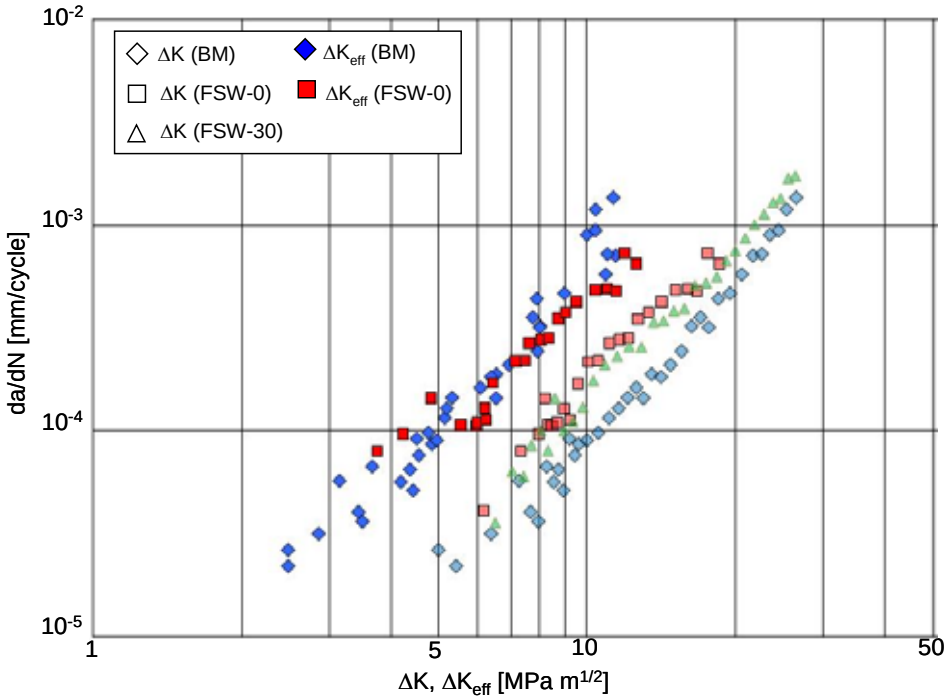

Figure 12.5 d*a*/d*N*-Δ*K* curve of FSW Specimens

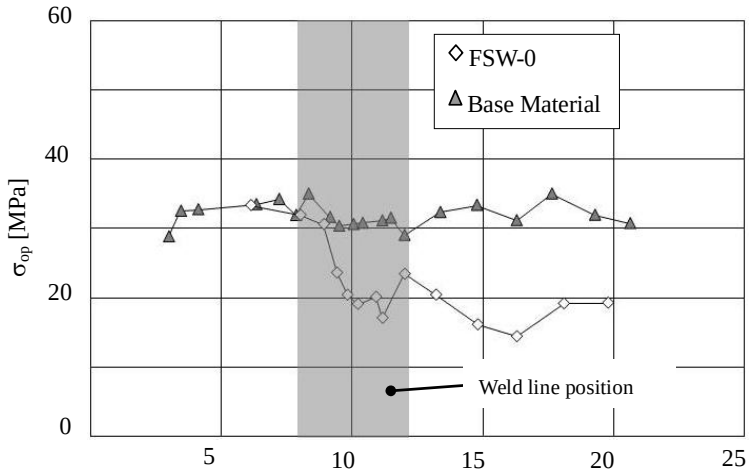

Figure 12.6 Crack Opening Stress with respect to Half Crack Length

Table 12.1 Surface Treatment Conditions

as weld	No additional surface treatment
both surface grinding	0.2mm grinding on both surface, Ra=25μm
top surface polished	Welding surface polished (up to 0.05μm)
both surface polished	Both surface polished (up to 0.05μm)

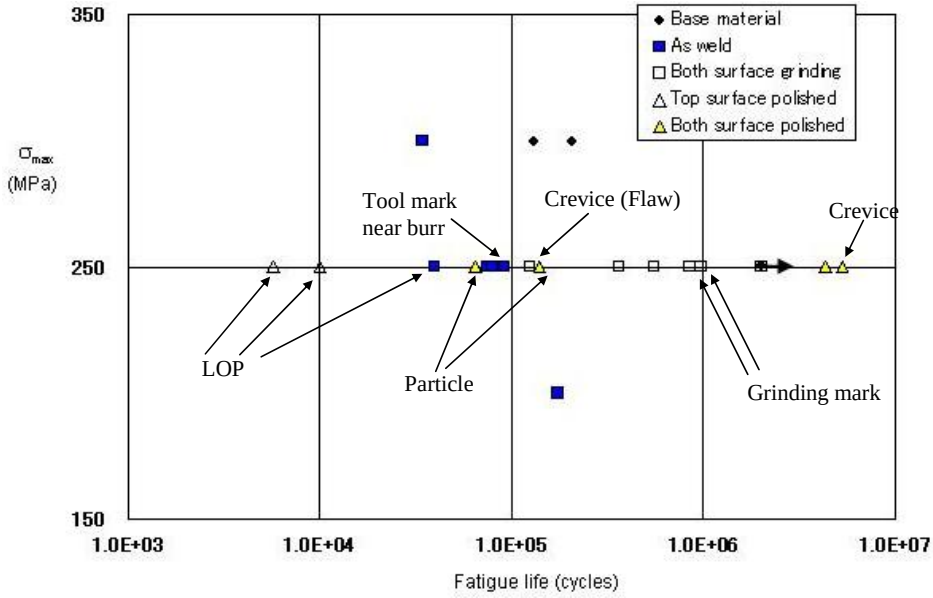

Figure 12.7 Fatigue Test Results of FSW Specimens with Different Surface Treatments

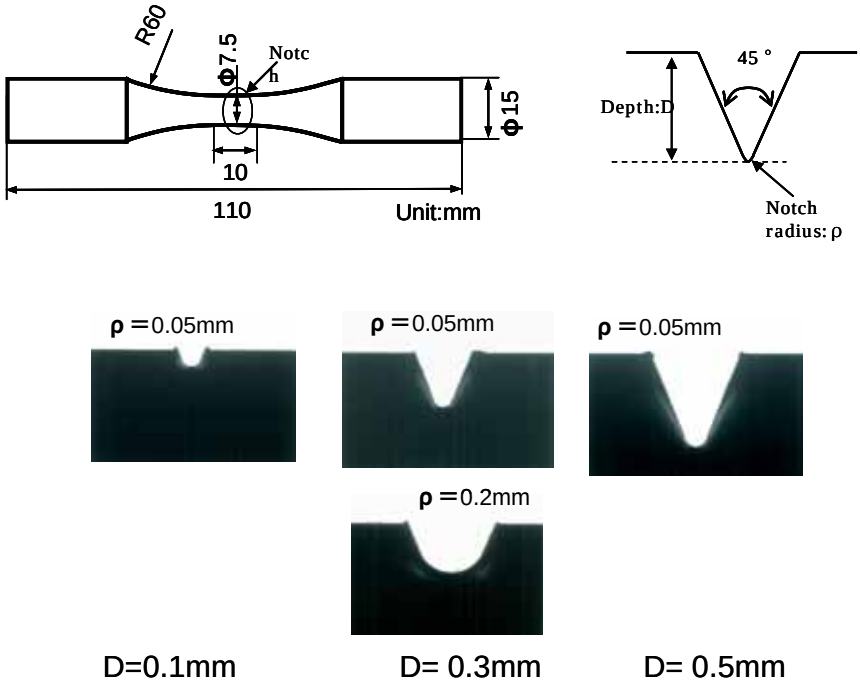

Figure 12.8 Fatigue Test Specimens

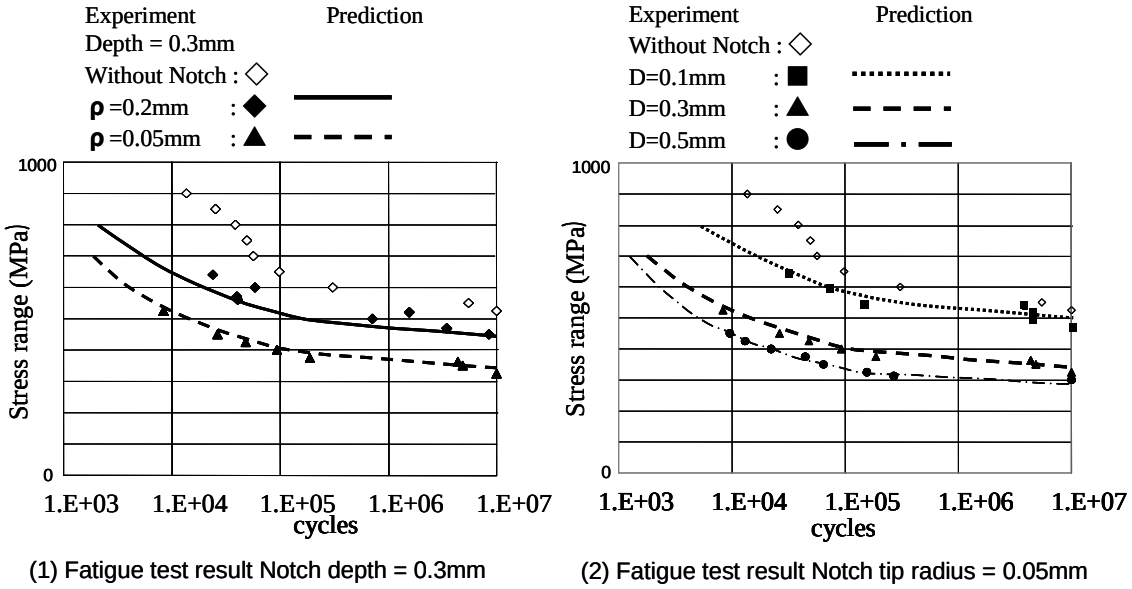

(1) Fatigue test result Notch depth = 0.3mm

(2) Fatigue test result Notch tip radius = 0.05mm

Figure 12.9 Comparison Between Experiments and Prediction with TCD

Table 12.2 Summary of Test Program of Mar-M247/IN-718 Dissimilar Metals

Specimen	Test	Test temperature (℃)	Phase angle (°)	Strain range	Strain ratio	Strain rate (/sec)	Hold time (sec.)	Remarks
IN-718	LCF	650	-	1.2～0.4	-1	5x10^ -4	0	F-F
	LCF			0.6～1.0	-1	5x10^ -4	600	Tension hold
	LCF			0.6～2.0	-1	2x10^ -5	0	S-S
Mar-M247	LCF	650	-	0.4～1.0	-1	5x10^ -4	0	F-F
	LCF			0.4～1.0	0		0	F-F
M247/IN718	LCF	650	-	0.5～1.2	-1	5x10^ -4	600	Tension hold
	LCF			0.6～1.0	-1	2x10^ -5	0	S-S
	TMF	300/650	180	0.6～1.0	-1	2x10^ -5	0	OP TMF
			0	0.6～1.0	-1	2x10^ -5	0	IN TMF

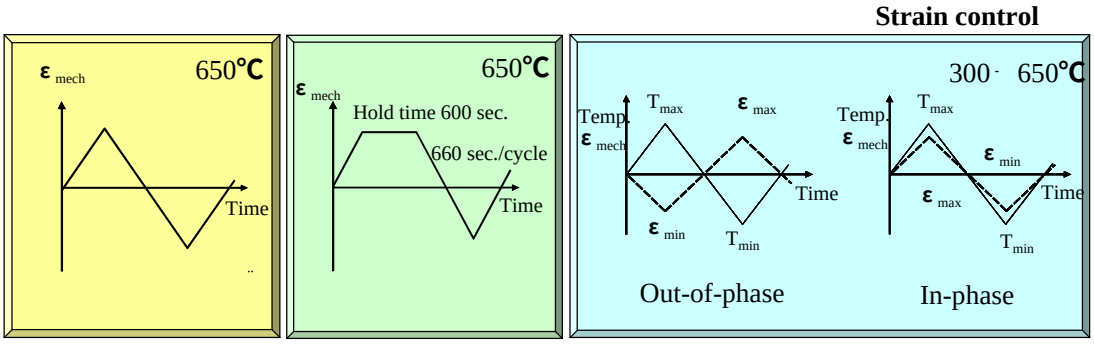

Low cycle fatigue(F-F nad S-S)

Creep-fatigue

Thermo-mechanical fatigue

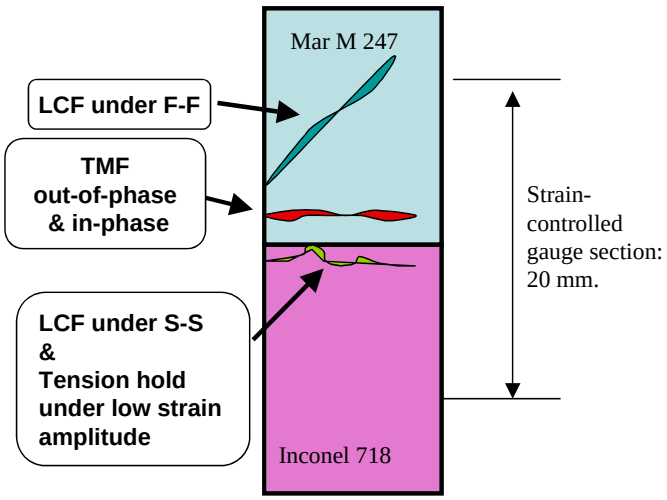

Figure 12.10 Illustrations Showing Both the Strain Gradient Controlled Test and the Failure Modes Depending on Loading Modes

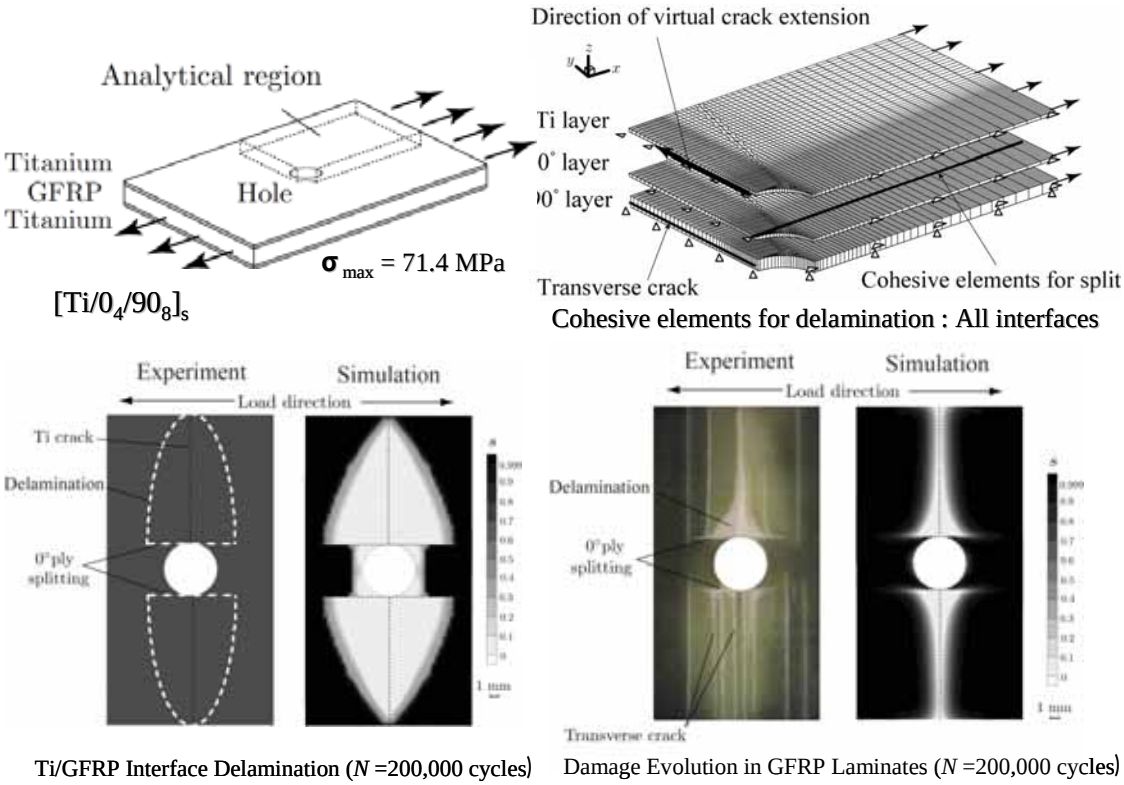

Fig. 12.11 Comparison of Theoretical Prediction with Experiments for Damage in Ti/GFRP laminates

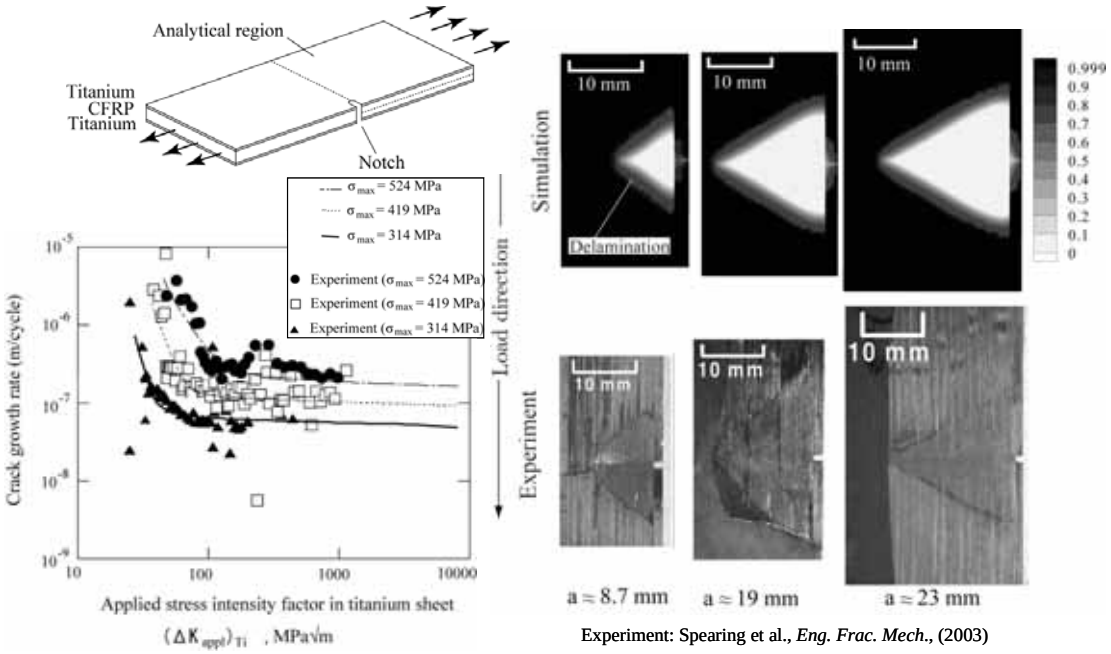

Experiment: Spearing et al., *Eng. Frac. Mech.*, (2003)

Fig. 12.12 Comparison of Theoretical Prediction with Experiments for Damage in Ti/CFRP laminates

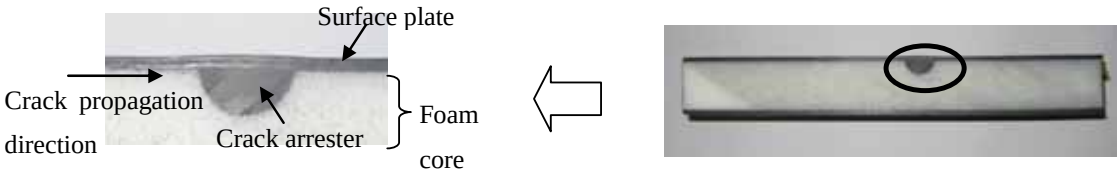

Figure 12.13 Crack Arrester Concept

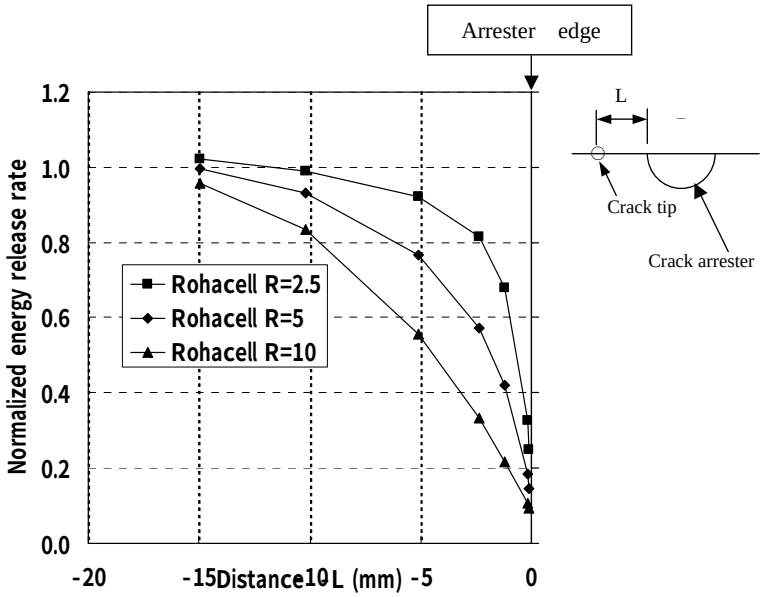

Fig. 12.14 Relation between Energy Release Rate *G* and Distance *L* for Mode I Type Loading (*P* = 0.28 N/mm)

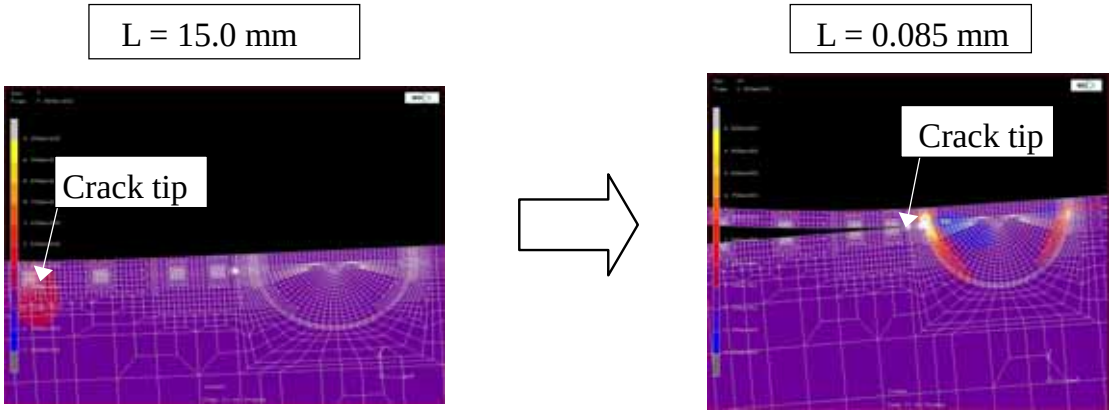

Fig. 12.15 Distributions of σ_{yy} for Mode I Type Loading Condition (Arrester Radius: 5 mm, *P* = 28 N)

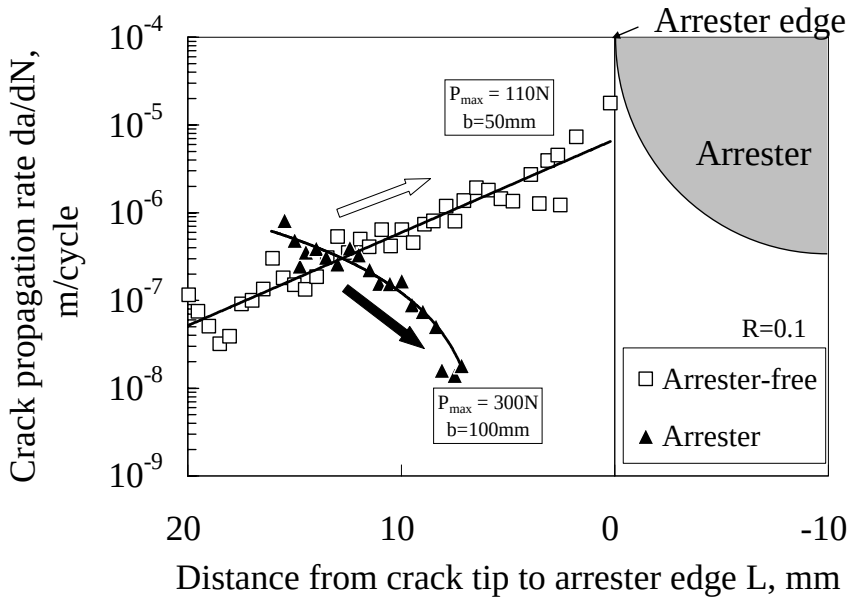

Figure 12.16 Relation between Crack Propagation Rate d*a*/d*N* and Distance from Crack Tip to Arrester Edge under Mode I Type Loading

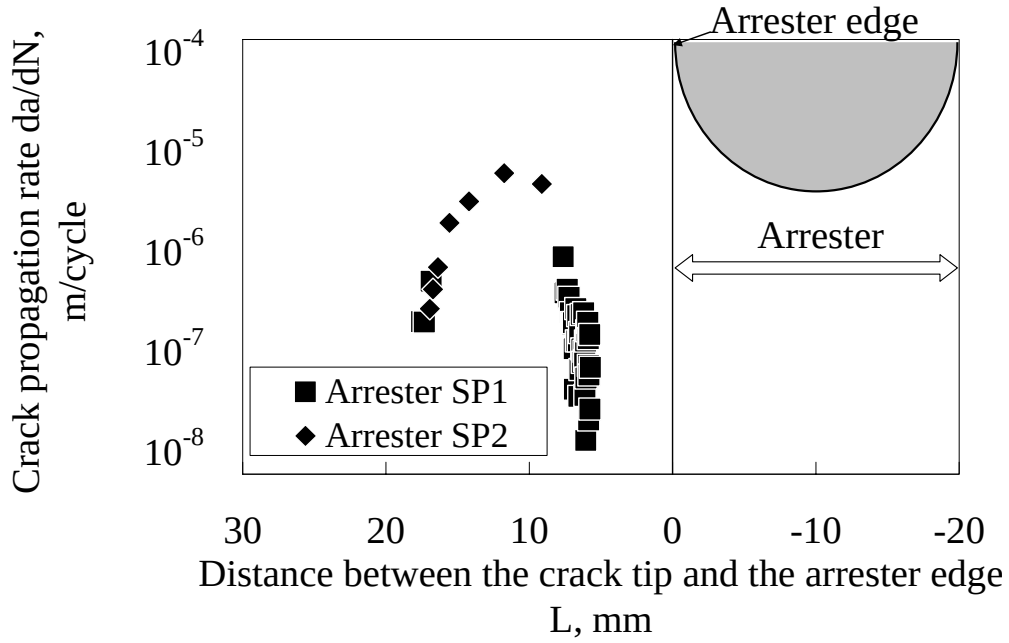

Figure 12.17 Relation Between the Crack Propagation Rate, d*a*/d*N* and Distance from Crack Tip to Arrester Edge, *L* under Mode II Type Loading

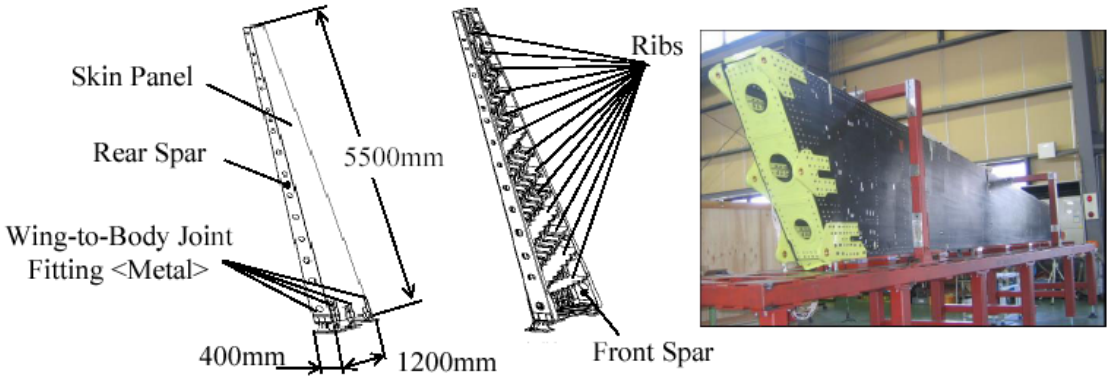

Fig. 12.18 Full-Scale Vertical Stabilizer Box Fabricated with A-VaRTM Process

Fig. 12.19 Test Setup of Full-Scale Vertical Stabilizer Box

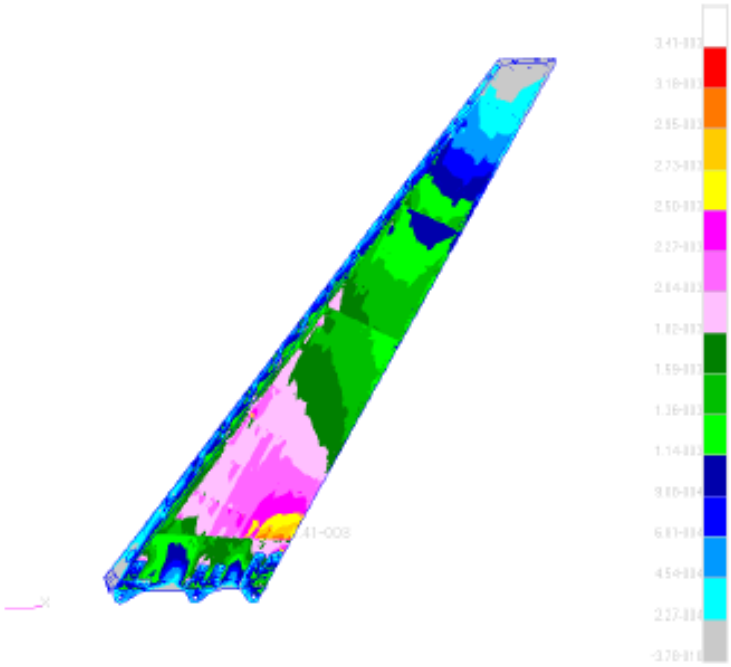

Fig. 12.20 FEM Analysis Results (Strain Distribution)

Figure 12.21 Next-generation Maritime Patrol Aircraft (XP-1)

Figure 12.22 Next-generation cargo transport (C-X)

Fig. 12.23 Model YS-11A-500

Table 12.3 Specification and Performance of Model YS-11

Length Overall	26.3m	
Wingspan	32.0m	
Height	8.98m	
Fuselage Diameter	2.88m	
Type	YS-11-100	YS-11A-200/-500
Max. Take-off weight	23,500kg	24,500kg/25,000kg
Crew	2	
Passenger	Max. 64 (Standard 60)	
Max. Payload	5,635kg	6,538kg/7,038kg
Powerplant (Twin)	Rolls-Royce Dart Mk 542-10 or -10J or -10K	
Propeller	Dowty Rotol (c) R209/4-40-4.5/2	
Cruising speed (15,000ft)	258kt	255kt
Range	1,250nm	1,230nm/1,210nm
Max. Operating Altitude	20,000ft	
Take-off Distance	970m	1,110m/1,310m
Landing Distance	1,070m	1,100m/1,110m

Table 12.4 Items in AC25.271-1C to be Determined Specific Solution

Design and Evaluation	Identificationn of components to be evaluated Identification of principal structural elements Selection of critical damage areas
Damages and Defects	Identification of damage location to be evaluated Selection of damage type and size
Tests	Comparability of Loads Spectrum between tests and actual flight Comparability between test articles and actual structure Determination of test cycles Method of artificial damage
Destructive Tests	Tear-down inspection method
Analysis	Validation of damage growth analysis methods and residual strength analysis methods
Inspection Methods	Determination of probability of Detection Determination of minimum detectable damage size Establishment of Inspection Program

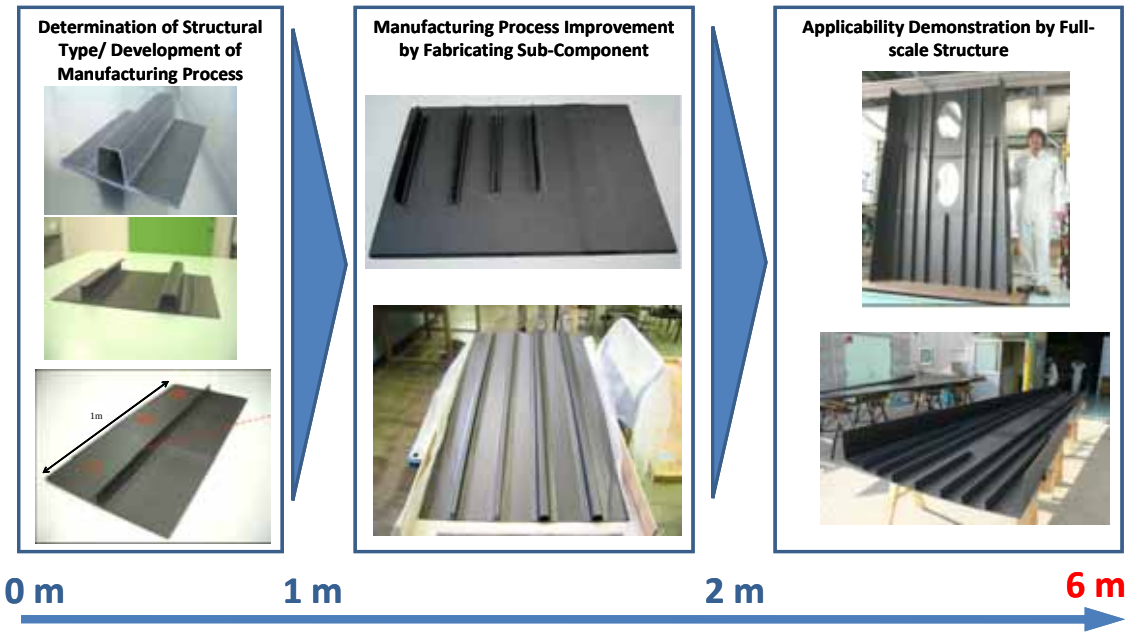

Figure 12.24 Schematics of Manufacturing Process Development Procedure

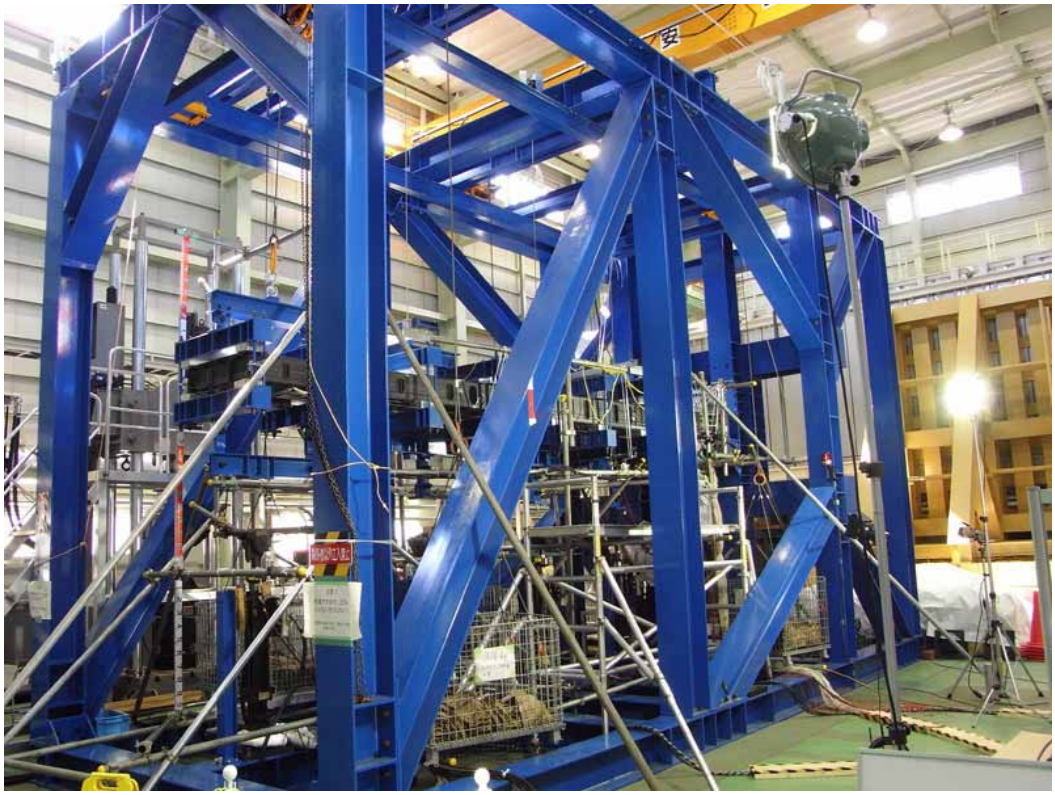

Figure 12.25 Experimental Setup for Full-scale Static Test

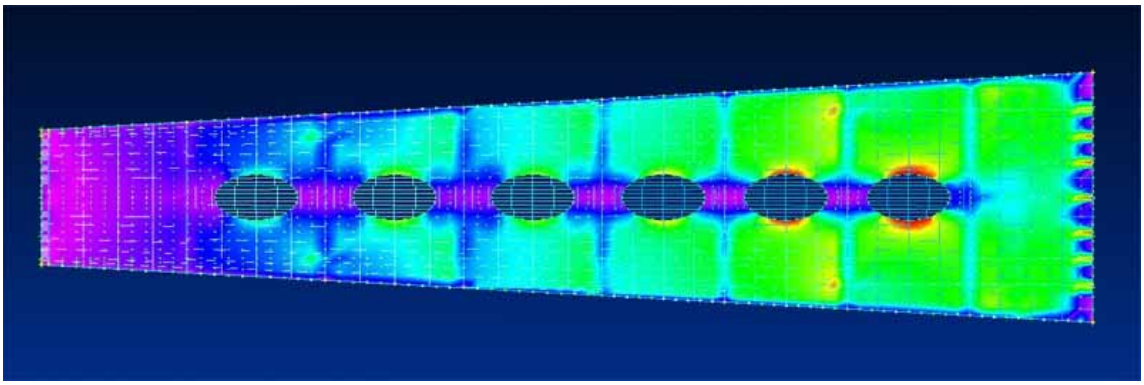

Figure 12.26 FEA Prediction of Strain Distribution (Lower Skin)

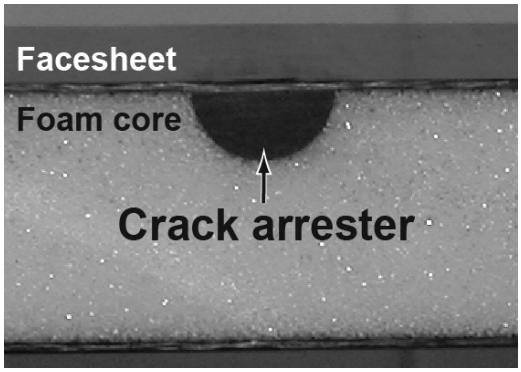

Figure 12.27 Crack Arrester

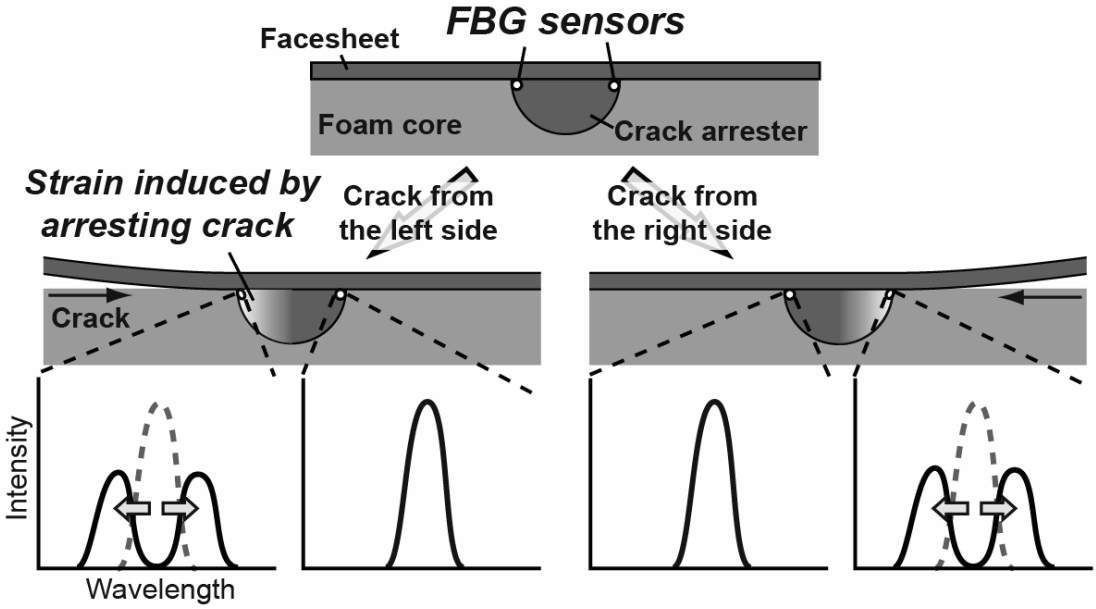

Figure 12.28 Schematic of crack detection technique.

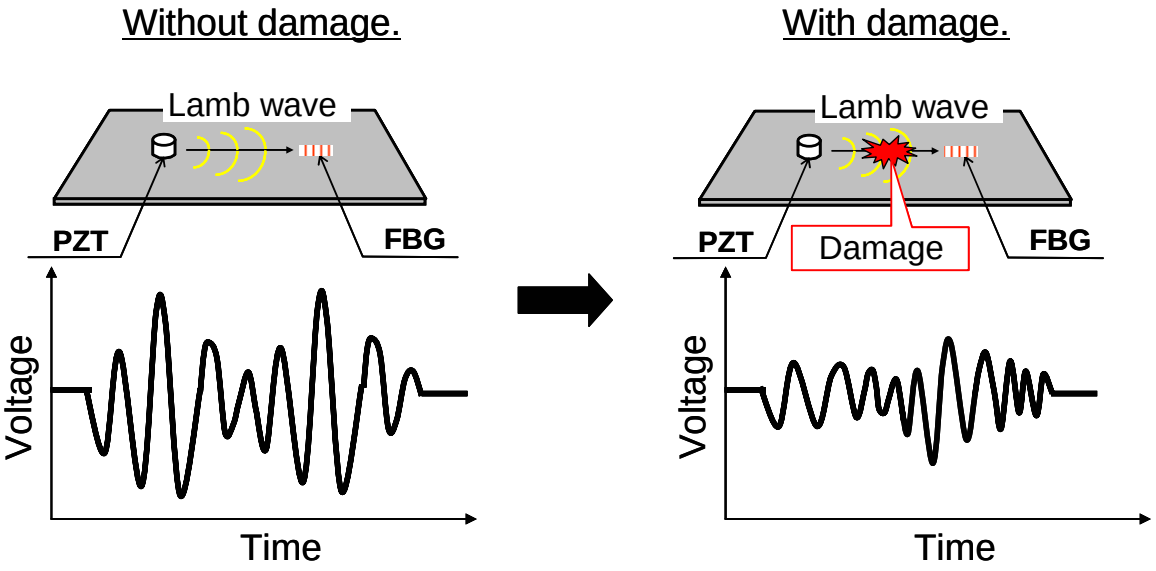

Figure 12.29 Schema of Position of FBG Sensor and PZT Actuator and

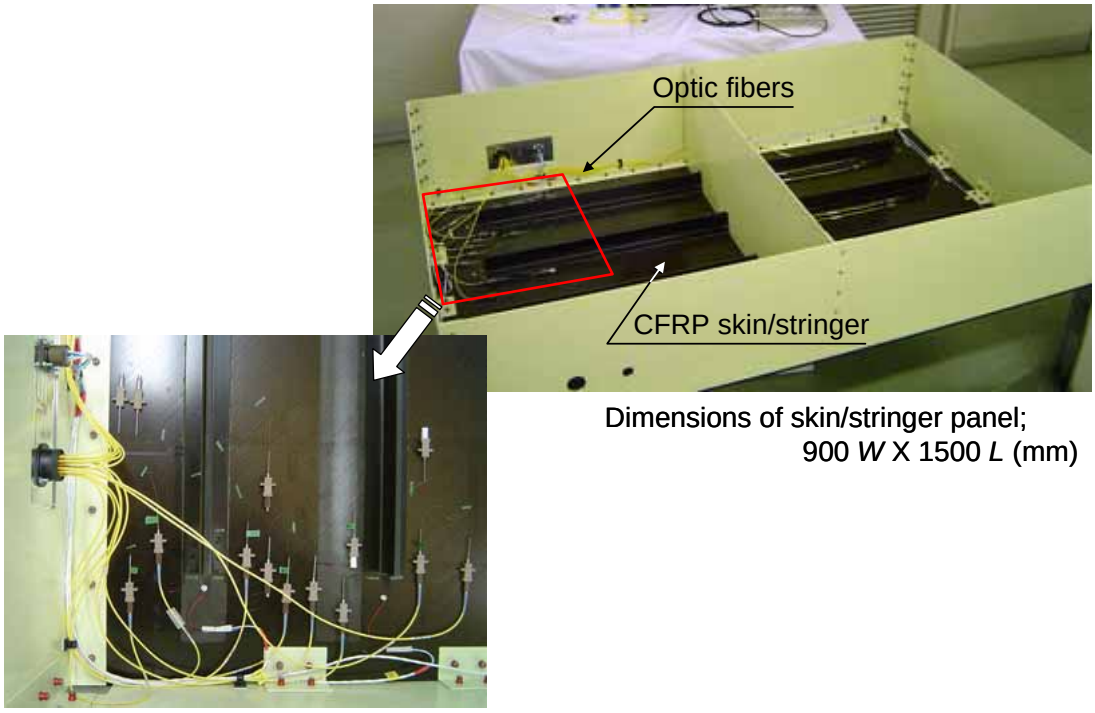

Figure 12.30 Schema of Sub-component Test Article

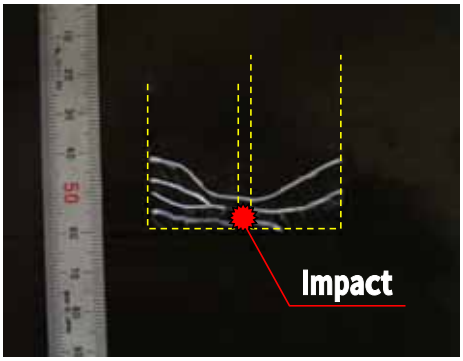

Damaged area inspected by A-scan

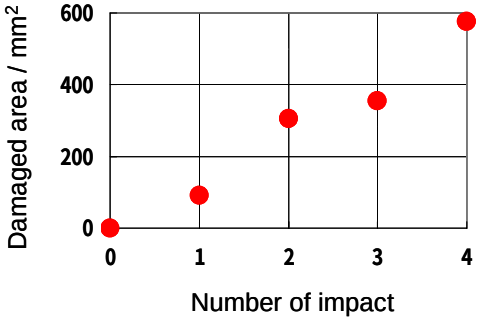

Relationship between number of impact and damaged area

Figure 12.31 Results of A-scan Inspection

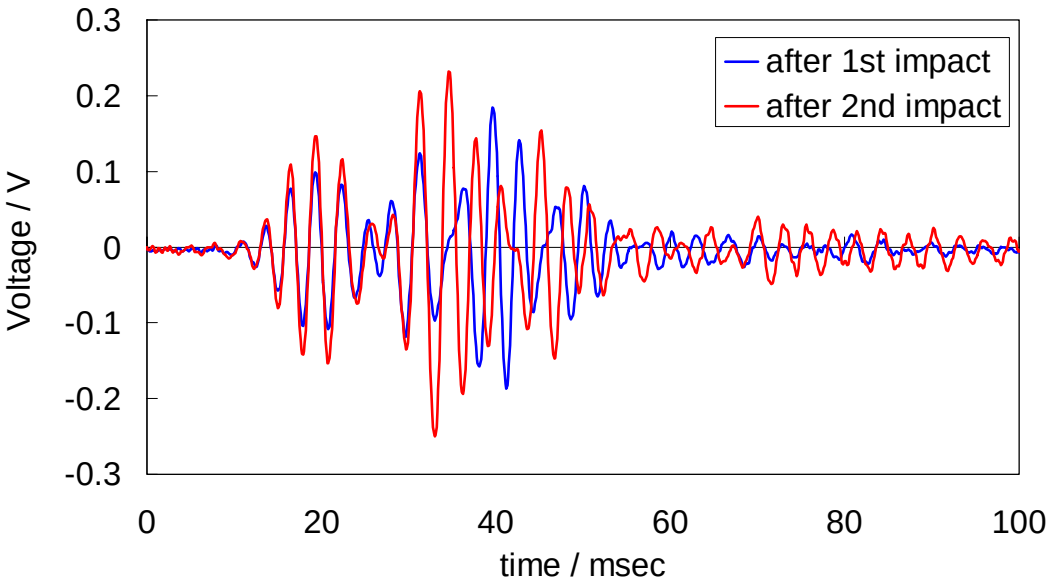

Figure 12.32 Examples of detected Lamb Wave (Bonded FBG sensor)

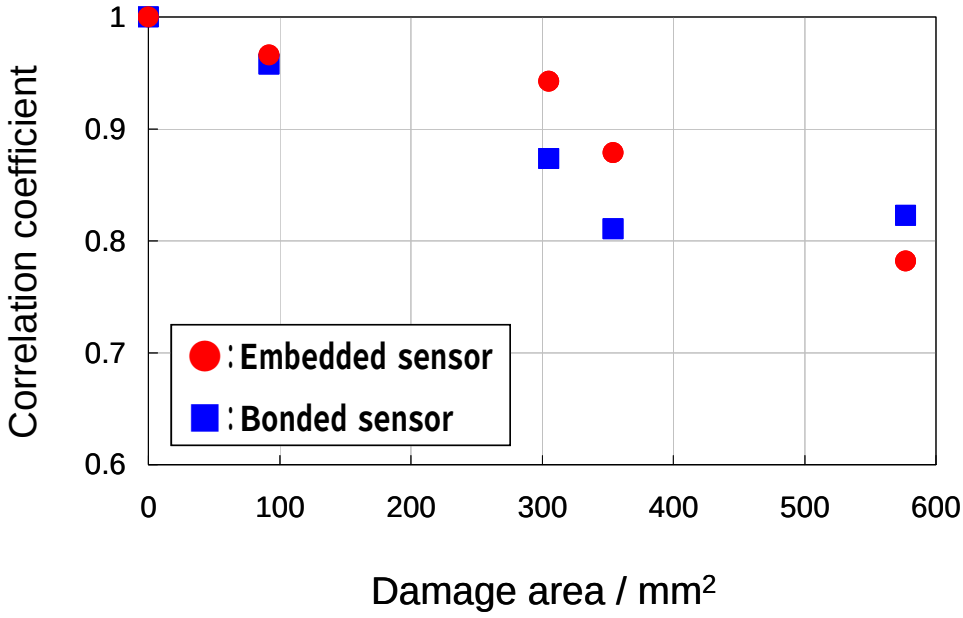

Figure 12.33 Relationship between Correlation Coefficient and Damaged Area

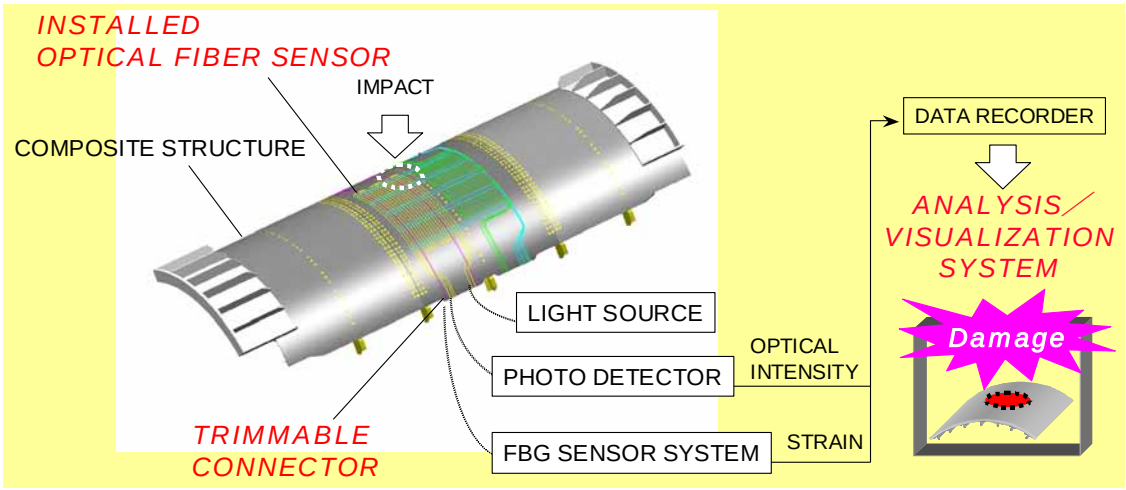

Figure 12.34 Impact Damage Detection System

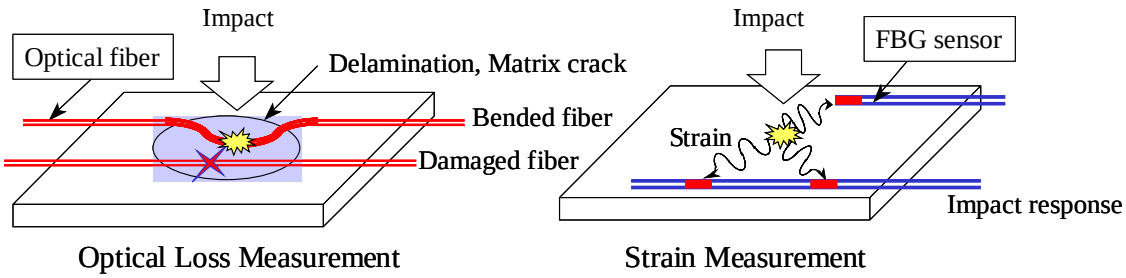

Figure 12.35 Measuring Principle

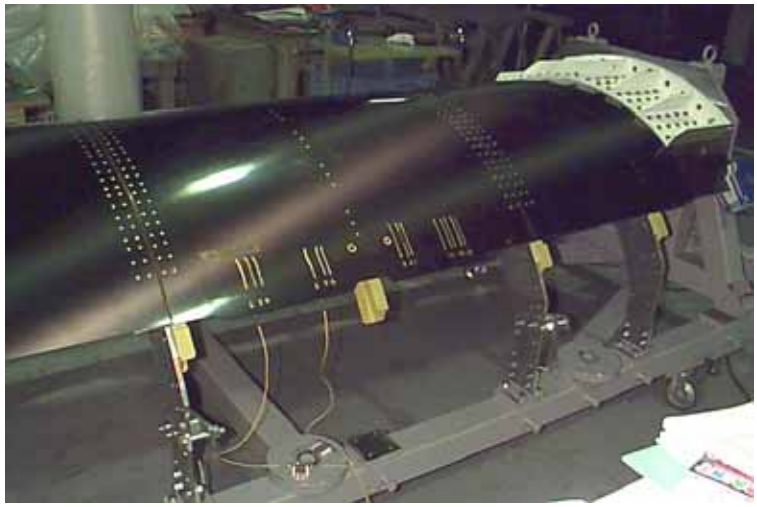

(a) Upper Panel with Embedded Optical Fiber Sensors and Trimmable Connectors

(b) Appearance of Test System

Figure 12.36 Composite Fuselage SHM Demonstrator Test

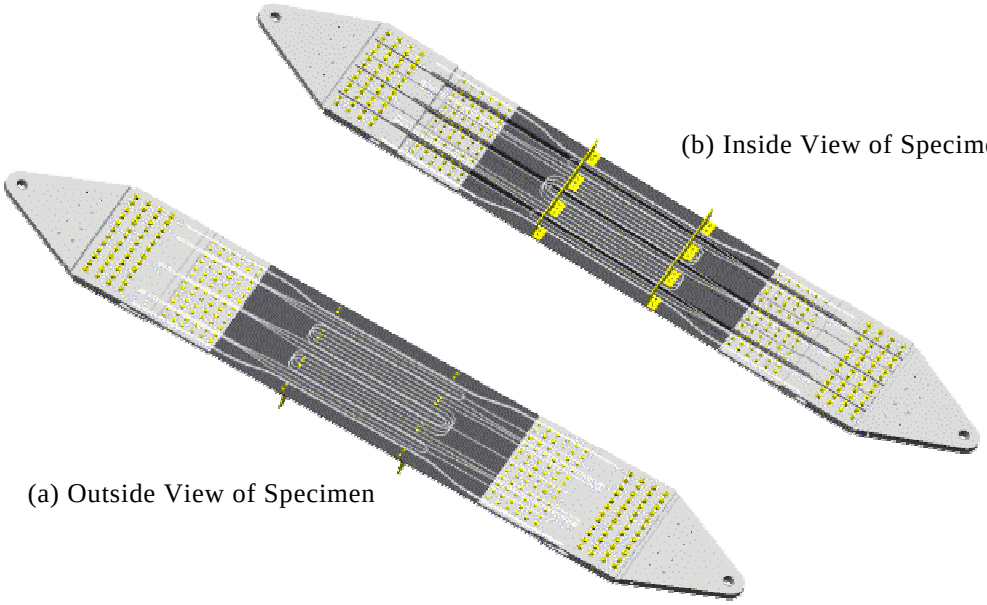

(b) Inside View of Specimen

(a) Outside View of Specimen

* White line indicates embedded small-diameter optical fibers.

Figure 12.37 Stiffened Panel with Fittings

(a) Test System for Impact Loading Test

Figure 12.38 System Evaluation Test

(b) Test System for Cyclic Loading Test

Figure 12.38 System Evaluation Test (Continued)

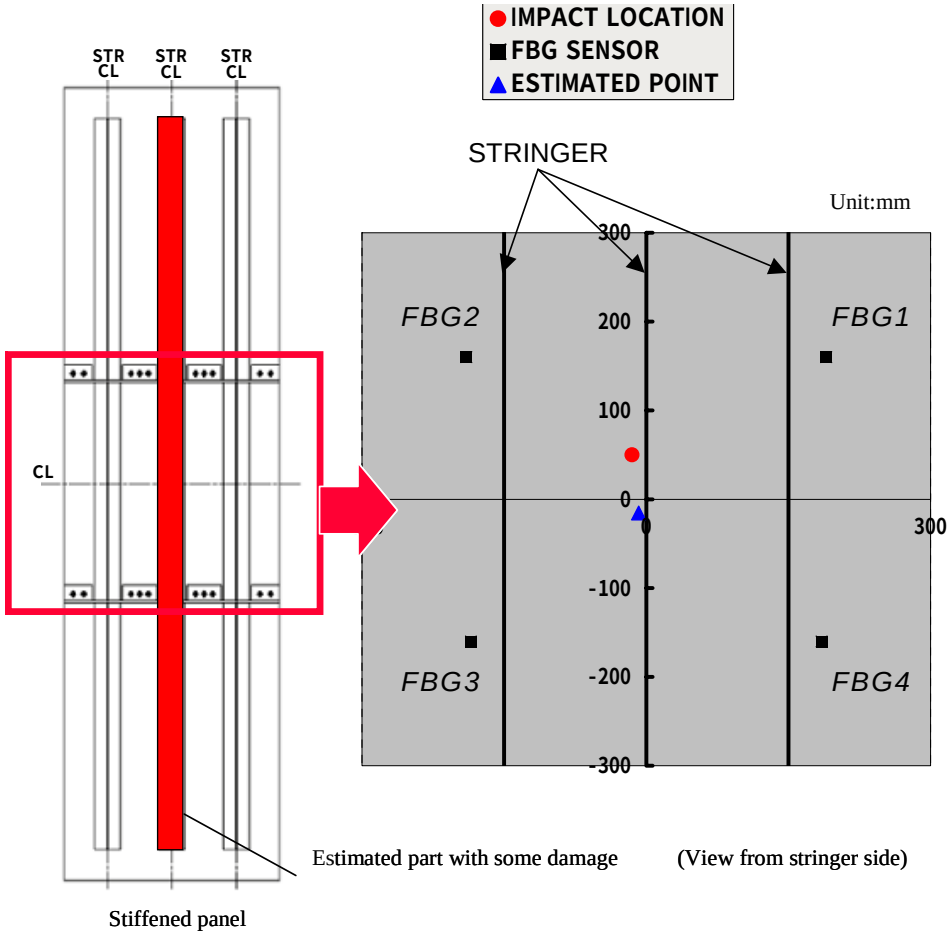

Figure 12.39 Impact Identification Test Result

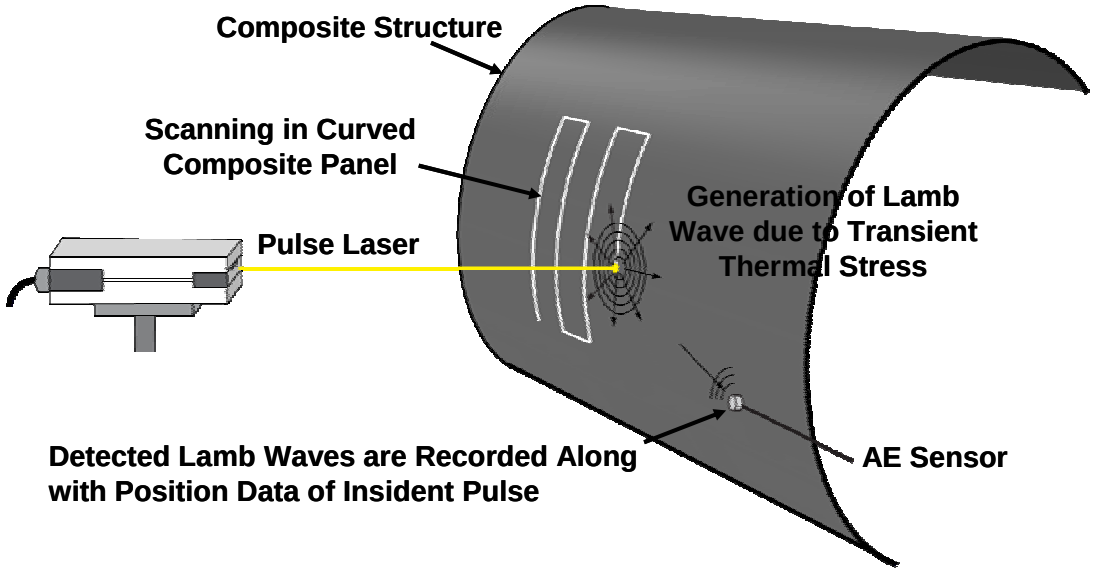

Figure 12.40 Full-Field Damage Detection System Using Pulse-Laser Generated Lamb Waves

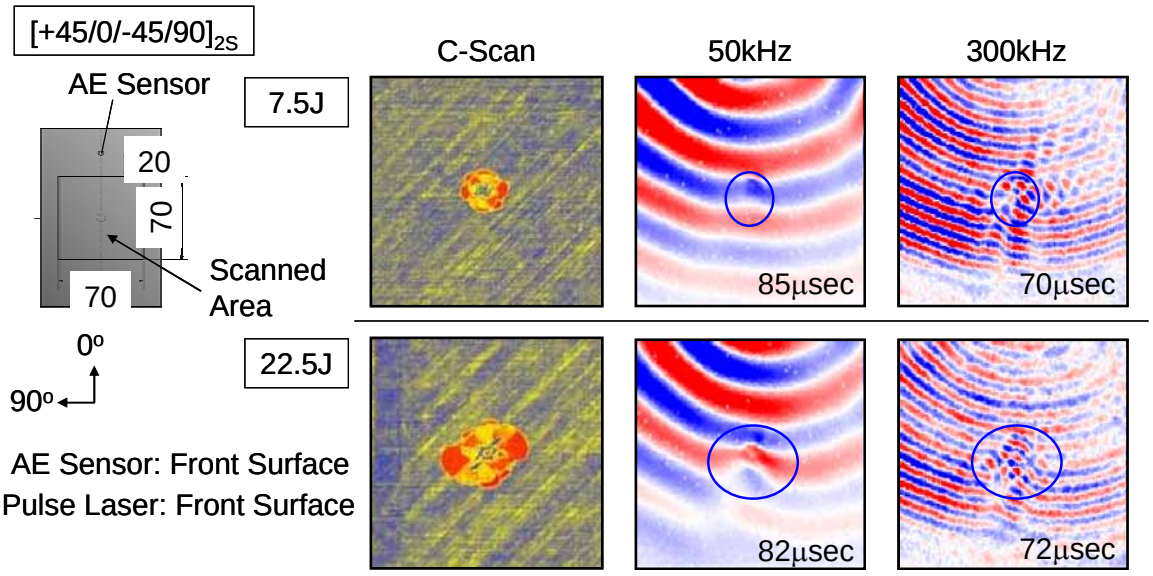

Figure 12.41 Visualized Lamb Wave Propagation along with C-scanned Images of Impact-induced Delamination Patterns in Quasi-isotropic Composite Laminates

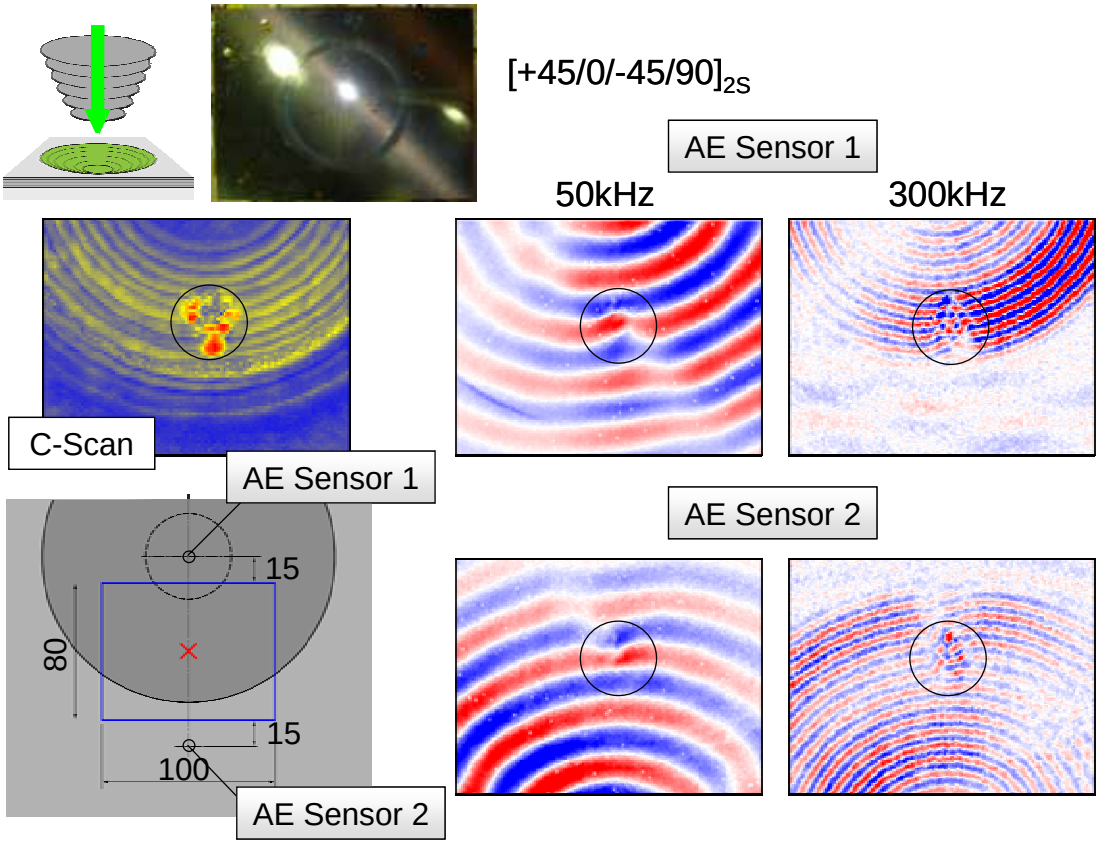

Figure 12.42 Detected Impact-Induced Delamination in Repaired Quasi-isotropic Composite Laminates

Table 12.5 Number of Accident Causes by Factor

Category / Year	Pilot	Maintenance or Material	Weather or other reason	Still under investigation	Total
2007	12	1	7	3	23
2008	0	0	1	16	17

Table 12.6 Number of Serious Incident Causes by Factor

Category / Year	Pilot	Maintenance or Material	Weather or other reason	Still under investigation	Total
2007	4	1	4	3	12
2008	0	0	0	5	5

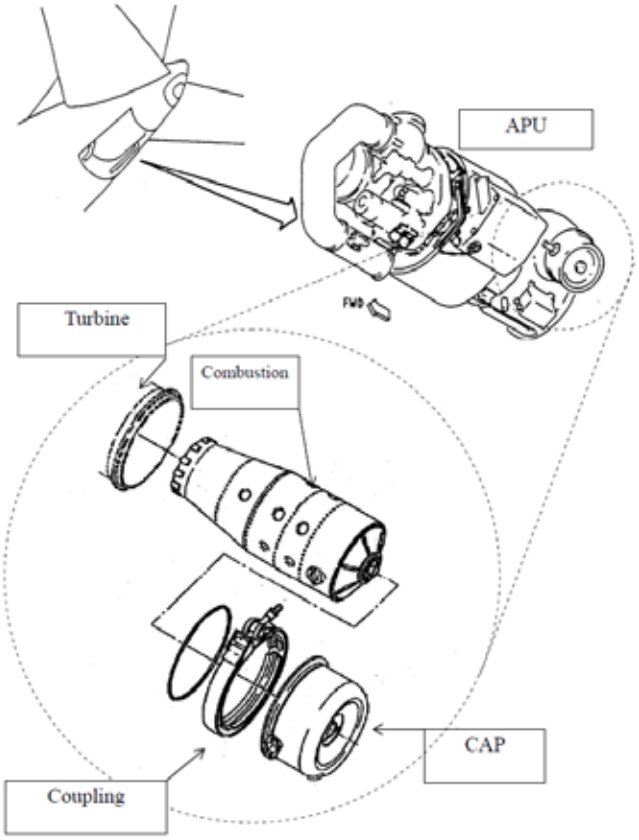

Figure 12.43 Coupling in APU

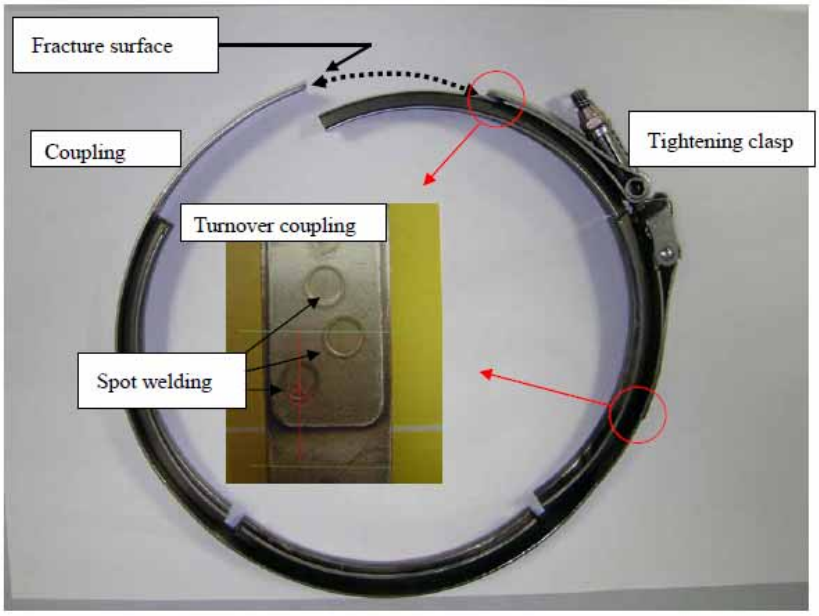

Figure 12.44 Fractured Coupling